ResearchGate

See discussions, stats, and author profiles for this publication at: https://www.researchgate.net/publication/231654197

Self-Assembled Monolayer Islands Masked Chemical Etching for Broad-Band Antireflective Silicon Surfaces

ARTICLE *in* THE JOURNAL OF PHYSICAL CHEMISTRY C · JANUARY 2010

Impact Factor: 4.77 · DOI: 10.1021/jp908139h

CITATIONS
15

READS
20

6 AUTHORS, INCLUDING:

Nan Lu
Jilin University
73 PUBLICATIONS **1,405** CITATIONS
SEE PROFILE

Lifeng Chi
Soochow University (PRC)
337 PUBLICATIONS **6,367** CITATIONS
SEE PROFILE

Available from: Lifeng Chi
Retrieved on: 23 January 2016

Self-Assembled Monolayer Islands Masked Chemical Etching for Broad-Band Antireflective Silicon Surfaces

Wen-Tao Wang,[†] Nan Lu,*[,†] Juan-Yuan Hao,[†] Hong-Bo Xu,[†] Dian-Peng Qi,[†] and Li-Feng Chi*[,†,‡]

State Key Laboratory of Supramolecular Structure and Materials, College of Chemistry, Jilin University, 130012, Changchun, People's Republic of China, and Physikalisches Institut and Center for Nanotechnology (CeNTech), Westfälische Wilhelms-Universität, D-48149 Münster, Germany

Received: August 24, 2009; Revised Manuscript Received: December 29, 2009

We report a simple and low-cost nonlithographic approach to fabricate tapered silicon arrays for broad-band antireflective coatings. Wafer-scale, subwavelength-structured pyramidal arrays are directly patterned on Si using mixed self-assembled monolayers consisting of octadecyltrichlorosilane islands as KOH etching masks. We have investigated the effects of etching conditions (such as temperature and pH of solution and etching time) on antireflective properties. The reflectivity of Si surfaces can be suppressed to below 3.8% in the waveband of 300−2000 nm. This technique combines the simplicity of self-assembly and cost benefits of chemical etching, which is promising for reducing the manufacturing cost of crystalline silicon solar cells and optical devices.

Introduction

Antireflective (AR) coatings are of great scientific and technological interest, particularly in development of solar cells,[1,2] electrooptical devices,[3] and sensors.[4,5] More than 30% of incident light is reflected back from silicon (Si) surfaces by Fresnel reflection[6,7] because of the high refractive index of Si, which greatly reduces the conversion efficiency of photovoltaic devices. Conventionally, single- or multilayered thin-film coatings are used to achieve antireflection.

Although thin-film technology is widely used for the mass production of AR coatings on different surfaces, the process has some problems, such as adhesion, thermal mismatch, and thin-film stack stability.[8,9] Meanwhile, for single-layered coatings, the following conditions are needed:[10,11] (a) the thickness of the coating is $\lambda/4$, where λ is the wavelength of incident light, and (b) an ideal homogeneous single-layer AR coating satisfies the following condition, $n_C = (n_A n_S)^{1/2}$, where n_C, n_A, and n_S are refractive indices of the coating film, air, and substrate, respectively. Most glass materials have an index of refraction between 1.45 and 1.65 in the visible spectral region, which implies that the index of refraction of the antireflective interference film must be between 1.20 and 1.25.[12] Such a low-index requirement makes it practically impossible to design a dense single-layer AR film on glass because of the low refractive index without any known coating material matched with it.[13]

Inspired by the microstructured cornea of some nocturnal moths,[14,15] subwavelength structures (SWSs) directly patterned on Si substrates have been extensively explored both experimentally[16−26] and theoretically[27−30] for developing broad-band AR coatings. Theoretical studies indicate that the subwavelength-structured (SWS) arrays, with the dimension smaller than the wavelength of a given incident light, can suppress the Fresnel reflection over a wide spectral bandwidth by introducing a continuous effective index gradient between the substrate and the surrounding medium.[21,27] Compared with optical thin-film AR coatings, SWS surfaces are more stable and durable because the AR structures are fabricated with a single material. SWS surfaces are also suitable for high-energy ultraviolet and infrared applications where the thin-film optical AR coatings may not exist.[28] Over the past decade, many texturing techniques for fabricating SWS surfaces have been proposed, including mechanical diamond saw cutting,[17] electron-beam lithography,[18] laser interference lithography,[19,20] nanoimprint lithography,[21,22] reactive ion etching,[23] and self-assembly.[24−26] Unfortunately, these top-down nanolithographic techniques are highly restricted by factors, such as mask costs, complicated procedures, and inefficient processing.[25,26,31] Most textured surfaces show satisfactory AR coating only over a wavelength around 500−900 nm,[32] while the reflectance in the near-infrared range can only be reduced by 60%−70%.[19]

Jiang et al.[25] have utilized spin-coated monolayer colloidal crystals as shadow masks to generate metallic nanohole arrays. Inverted pyramid arrays in Si can then be generated by anisotropic wet etching with the nanohole template. Though the normal-incidence reflection (∼2 to 10%)[25] from the pyramid gratings is higher than other SWS AR coatings made by lithographic techniques, the cost benefit of this nonlithographic technique is a major advantage. For practical applications, however, techniques to fabricate broad-band antireflective SWSs with fewer procedures and lower cost are still highly sought after. In our previous work,[33] we reported a method to fabricate high-density antireflective pyramidal structures on single-crystal Si substrates, which are formed by an anisotropic KOH etching of the Si substrate with a Langmuir−Blodgett monolayer consisting of domain structures as masks. By means of the Si pyramidal structures, the reflectivity of a bare Si wafer is reduced to less than 6% from above 35% at the wavelengths from 400 to 2000 nm.[33]

In the present study, a simpler and more efficient fabrication technique in creating a wafer-scale SWS surface on a Si substrate is demonstrated. On the basis of the combination of

* To whom correspondence should be addressed. E-mail: luenan@jlu.edu.cn (N.L.), chi@uni-muenster.de (L.-F.C.). Fax: +86-431-85168477. Phone: +86-431-85168477.
† Jilin University.
‡ Westfälische Wilhelms-Universität.

10.1021/jp908139h © 2010 American Chemical Society
Published on Web 01/20/2010

self-assembly technique and wet etching of Si, pyramidal arrays are produced using an anisotropic KOH etching with the masks of solid-like octadecyltrichlorosilane (OTS) islands. The fabricated Si pyramids possess a continuous refractive index gradient from air to substrate. The reflectivity of polished Si was decreased to below 3.8% from 35% by means of the Si arrays.

Experimental Section

Chemicals. *n*-Octadecyltrichlorosilane (OTS, 90+% purity) and *n*-octyltrimethoxysilane (OTMS, 96% purity) were purchased from Sigma Aldrich Co. Analytical reagent-grade toluene, ethanol, acetone, chloroform, hydrogen peroxide, potassium hydroxide, ammonium hydroxide, and concentrated sulfuric acid were all purchased from the Beijing Chemical Works. The toluene was dried over sodium and heated at reflux for 5 h before being distilled. Other chemicals were used as received without any further purification. One side polished n-type (100) oriented Si wafer with a resistivity of 0.008−0.02 Ω·cm was purchased from GRINM semiconductor materials Co. Ltd., Beijing, China.

Preparation of Si Substrates. Si substrates used for self-assembled monolayer (SAM) growth in this research were cut from n-type (100) wafers. The slides were cut into pieces of appropriate size (1 × 1 cm^2 for AFM measurement, 2 × 2 cm^2 for spectra measurement). The Si substrates were subsequently sonicated in acetone, ethanol, and deionized water for 5 min to remove organic contaminants. The Si slides were then chemically oxidized with an alkali treatment (mixture of NH_4OH, H_2O_2, and H_2O with a volume ratio of 1:1:5, respectively) for 30 min at 80 °C, followed by etching in 10:1 deionized water/HF solution for 10 s to remove the native oxide layer completely, and finally reoxidized in a peroxy−sulfuric acid solution (3:1 mixture of H_2SO_4 and 30% H_2O_2) for 30 min at 80 °C. After they were sonicated in deionized water for 5 min and rinsed with successive water, the substrates were kept under deionized water (no longer than 2 h) and blow-dried in high-purity nitrogen just before use. This treatment results in a clean, new oxidized surface possessing the same topography as the original wafer.

Preparation of SAMs. The preparation of the adsorbate solutions and the film adsorption were carried out in a normal chemistry lab. The relative humidity was about at 6−8%. Mixed solutions of OTS (0.5 mM) and OTMS (0.5 mM) were freshly prepared in a solvent of toluene in order to reduce the amount of polymeric silane aggregates in the solution. To grow liquid-condensed (LC) islands, the mixed SAM adsorption reaction was allowed to proceed for 65 s at 8 °C, well below the critical temperature for the LC phase in the solutions.[34] Pure OTS SAMs were prepared at 8 °C for 65 s in 0.5 mM OTS solution; OTMS SAMs were prepared at the same conditions in 0.5 mM OTMS solution. Following adsorption, samples were withdrawn from the silane solutions and residual nonadsorbed silanes were removed from the substrate by immediately quenching in a stirred chloroform bath for 3 min and then blow-drying with nitrogen. This preparation procedure appeared to effectively remove excess polymer silane aggregates from the surface and yield well-formed LC OTS islands on a silica background.[35]

Preparation of SWS Coating. A plastic beaker with a magnetic stirrer was used as an etching bath; a hot plate with a temperature control probe was used for the bath heating. Etching was carried out by immersion of the sample in the KOH solution. In our experiments, etching processes were carried out with different temperatures and pHs of solution and etching times, which are discussed in detail in the following sections. The height of the produced Si arrays was controlled by etching duration. The sample was then rinsed with deionized (DI) water to remove KOH.

Characterization. Atomic force microscopy (AFM) was used for characterization of topography in ambient conditions at room temperature. The AFM instrument (Digital Instruments, Santa Barbara, CA) was operated in tapping mode using silicon nitride cantilevers (Nanosensors, Digital Instruments) with frequencies of 250−350 kHz. During operation, the AFM detected deflections of the probing cantilever by sensing the motion of a laser beam focused onto the backside of the cantilever. The feedback maintains a constant cantilever deflection. Scanning electron microscopy (SEM) micrographs were taken with a JEOL JSM 6700F field emission scanning electron microscope with a primary electron energy of 3 kV, and the samples were sputtered with a layer of Pt (ca. 2 nm thick) prior to imaging to improve conductivity. The reflection spectra were recorded at ambient temperature on a SHIMADZU UV3600 spectrophotometer with standard mirror optics in the range of 300−2000 nm. Contact angles (CA) were determined on a commercially available goniometer (DSA 10MK2, KRUSS) at room temperature. Water droplets of 3 μL were used for the contact angle (CA) measurements. At least five measurements were averaged for the CAs of the data reported here.

Results and Discussion

We prepared the mixed SAMs at $T = 8$ °C because it has been reported that the OTS-based monolayer forms by islands at $T < 16$ °C.[34,36,37] Figure 1a shows the AFM image of a mixed monolayer consisting of OTS islands on Si substrate. The scan size is 20 μm × 20 μm, and the scale bar is 10 nm. The average size of the island-like structures is around 1.0 ± 0.15 μm, which are surrounded by a flat, sealike region. These phase-separated films have been identified in previous publications:[38−42] the "islands" are composed of longer-chain components, while the "sea" is of shorter-chain components; the shorter-chain compounds are found to exhibit low contact angles. Island-like structures can be formed by OTS molecules because of a high lateral mobility of the adsorbed molecules and a two-dimensional condensation of ordered domains, driven by the attractive van der Waals interaction between the alkane chains of ca. 2 kcal/mol per methylene unit.[43] It is also supported by Monte Carlo calculations on the phase behavior in self-assembling alkane monolayers.[44] Due to weak intermolecular attraction between shorter chains, a sealike structure is formed by OTMS molecules.[41] Figure S1 (see the Supporting Information) shows the cross-sectional analysis of the mixed monolayer. The islands with the average height, $h = 1.8 \pm 0.1$ nm, were shorter than the length of a fully extended OTS chain (2.6 nm) and previous reported height.[34−37] However, Maboudian, R. et al[34,36,37] have reported that, for $T < 16$ °C, the OTS-based monolayer forms based on the island growth; the islands consist of fully extended chains, and essentially, no OTS molecules are found on the substrate between islands. It indicates that the height of OTS islands in our experiments should be about 2.6 nm. Actually, the observed height in section analysis is 1.8 ± 0.1 nm. We think that the difference is produced by the OTMS "sea", which filled the space of the islands. Additionally, the contact angle measurement technique is used to study the mixed monolayers. Figure 1b shows that the static contact angle for the mixed monolayer is about 97.1°, which is lower than that for pure OTS monolayers (99.4°) and higher than that for pure OTMS monolayers (61.5°) with a growth time of 65 s (see the

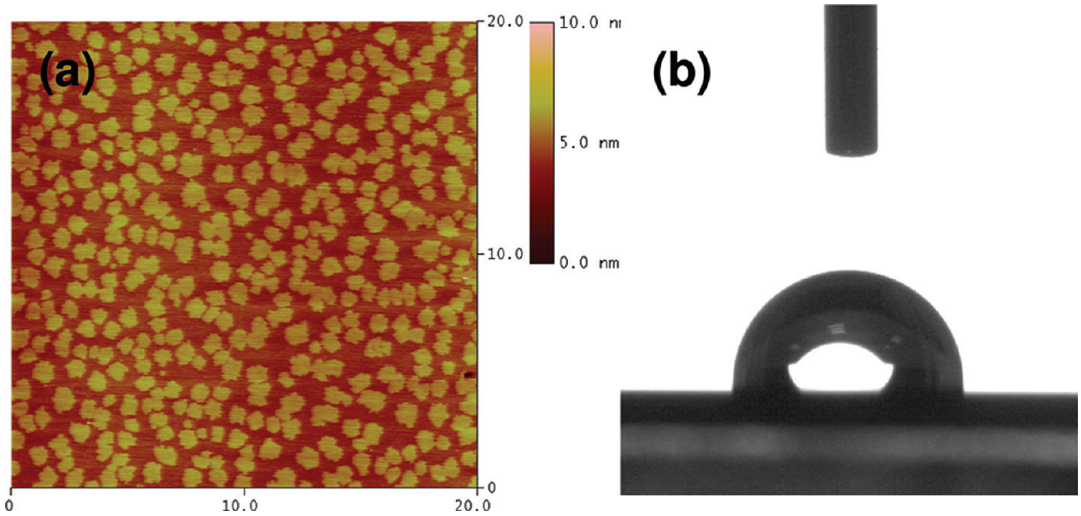

Figure 1. (a) AFM image and (b) static contact angle of the mixed monolayer containing OTS islands on a Si substrate. Scan size: 20 μm × 20 μm. The contact angle was measured to be about 97.1°.

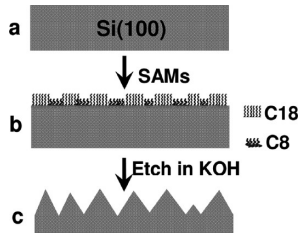

Figure 2. Schematic diagram of the fabrication process of the pyramidal arrays on a Si(100) wafer.

Supporting Information, Figures S5a and S6b). Water droplets of 3 μL were used for the contact angle measurements. At least five measurements were averaged for the data reported here. If the two components of a monolayer are to act independently, then the contact angles would follow Cassie's law:[45]

$$\cos \theta_{mix} = f_1 \cos \theta_1 + f_2 \cos \theta_2$$

where f_1 and f_2 are the fractions of the two components in the monolayer ($f_1 + f_2 = 1$) and θ_1 and θ_2 are the contact angles of the monolayers prepared with each individual component. The value of the θ_{mix} we calculated was 96.2°, in which the $\theta_1 =$ 107° for OTS,[46] $\theta_2 = 80°$ for OTMS,[47] and the surface coverage of OTS islands is about 60.5%. The calculated value is close to the experimental date. We think, in our experiments, the mixed monolayer is composed of solid-like OTS "islands" and a liquid-like OTMS "sea". This film is an ideal pattern mask for chemical etching to fabricate pyramidal arrays because the OTMS-covered regions can be selectively etched owing to their higher wettability and loose packing, whereas the close-packed, fully extended OTS-covered regions are protected because of their low wettability.[48,49] The fabrication process is schematically shown in Figure 2. First, a clean, hydroxylated silica surface was produced by a series of treatment, as described in the Experimental Section. Second, the mixed monolayers were transferred onto the substrate. The films consist of OTS "islands" and an OTMS "sea". The islands with fully extended chains were closely packed, while OTMS molecules were a disordered packing-like "sea", as shown in Figure 2b. The modified substrate was then etched in KOH solution, in which the OTMS-covered surfaces were selectively etched because of high wettability. Because of the different densities of Si atoms on Si(100) and Si(111),[50] the etch rate of Si(100) is much higher than that of Si(111), so pyramidal shapes were formed due to the characteristic 54.7° sidewalls, as shown in Figure 2c.

The formed OTS SAMs without OTMS at the same experimental conditions exhibit as fractal aggregates, which were branched islands (see the Supporting Information, Figure S5a), consistent with previous studies.[34−37,51,52] These islands were not as condensed as the circular OTS islands existing in mixed films, so they could not effectively protect covered regions from etching. Therefore, fractal islands were not suitable to be used as etching masks. This will be discussed in detail in the following section. Also, we prepared the SAMs of pure OTMS. As shown in Figure S6a (Supporting Information), the homogeneous film without phase separation was observed at the same experimental conditions. No islands were observed in the AFM image; however, the contact angle of water increased from 0° to about 61.5°. This suggested that a continuous film of disordered molecules adsorbed on the surface. In terms of weak intermolecular attraction for shorter chains, a liquid-like structure was formed by OTMS molecules.[42] Without a remarkable wettability difference, selective chemical etching was hardly to be realized with the OTMS monolayer as a mask. Therefore, the pure OTMS films cannot be used as etching masks.

We studied the effects of different anisotropic etching conditions on the pyramidal Si arrays. Figure 3 shows SEM images for the Si SWSs fabricated with different etching times in a KOH solution with a pH of 13 at 50 °C. The top-view SEM images shown in the left column reveal that the arrangement of the Si SWSs is the same as that of the original OTS islands. The shapes and density of the SWSs are also well consistent with those of the original OTS islands. The cross-sectional SEM images in the right column show that the etched sample presents an anisotropic angle of 54.7° (see Figure 3c), which is the characteristic KOH etching angle (the intersection of a (111) sidewall and a (100) plane of Si). The heights of SWSs of the samples etched for 10, 20, and 30 min are about 200, 550, and 800 nm, respectively. With increasing the etching time, V-shaped grooves between the SWSs become wider until the intersection of two Si(111) sidewalls (see Figure 2c). As the etching time is prolonged, the tops of the Si arrays change from flat to sharp after 30 min of etching and the height of SWSs increase to 800 nm from 200 nm.

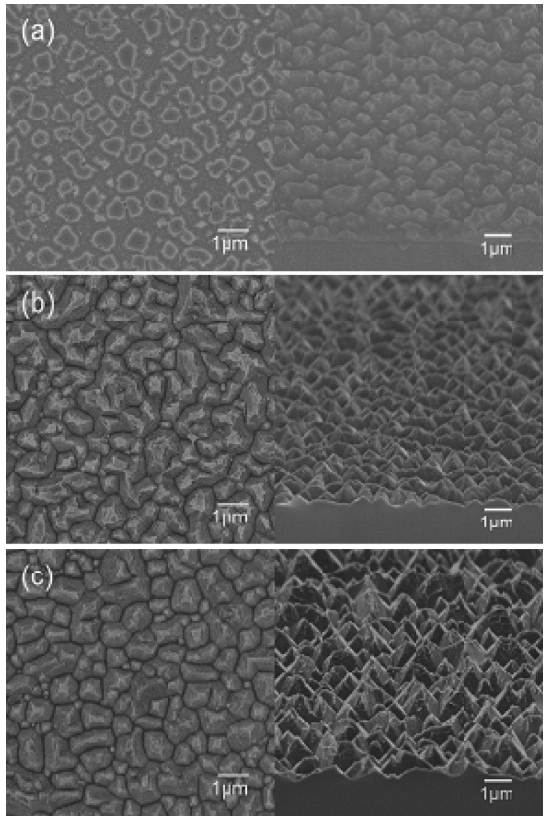

Figure 3. Top-view (left column) and cross-sectional (right column) SEM images for the Si arrays with different etching times in a KOH solution with a pH of 13 at 50 °C: (a) 10 min, (b) 20 min, and (c) 30 min.

As shown in Figure 4a, the photograph demonstrates the different antireflective behaviors of the SWS Si surface (right) and the polished Si surface (left). The polished Si wafer is mirror-like, while the pyramidal Si arrays (etched for 30 min) show dark black. The reflectance spectra of Si arrays are evaluated using visible−near-IR reflectivity measurement at normal incidence. Figure 4b shows the measured reflectivity for the etched samples in the waveband of 300−2000 nm. For the sample with 10 min of etching, the reflectivity is reduced to less than 16% in the whole measured waveband. For the sample with 20 min of etching, the reflectivity is below 6%. The reflectivity can be further reduced to below 3.8% in the wavelengths ranging from 300 to 2000 nm by 30 min of etching, which is a significant decrease for the polished Si (∼35%). The results suggest that lower reflectivity can be obtained by increasing the height of the Si arrays and tapering the arrays by prolonging the etching time. In Figure 4b, due to the wavelength change at 830 nm of the instrument itself, an undesired signal is produced. (Theoretically, no signal should be produced at 830 nm.)

When the etching experiments were carried out at room temperature (25 °C) and 38 °C in a KOH solution with a pH of 13, the samples also exhibit good AR performance in broad band. Figure 5b shows that the height of the pyramidal array produced by etching for 12 h at 25 °C is ∼750 nm. The reflectivity of Si can be decreased to below 5% (red dotted line in Figure 6) in the measured waveband, which is lower than those of the samples etched for 1 h (>32%) and 5 h (∼21%) in the same etching solution (see the Supporting Information, Figure S2). Figure 5c shows SEM images of the sample etched for 1 h at 38 °C. With 1 h KOH etching, the Si array exhibits a tapered shape. The reflectivity is reduced to below 3.2% (green dotted line in Figure 6) for a wide range of wavelengths, much lower than those of the samples etched for 10 min (>30%) and 30 min (∼14%) (see the Supporting Information, Figure S3). The effect of etching time on the created arrays has also been investigated in the KOH solution with a pH of 12 at 50 °C. A truncated array is obtained with 20 min of etching (Supporting Information, Figure S4a). When the etching time is extended to 50 min, a tapered array can be obtained (Supporting Information, Figure S4b). The reflectivity for the samples etched for 20 and 50 min are below 15% and 7% at the wavelengths ranging from 300 to 2000 nm, respectively (Supporting Information, Figure S4c). However, Figure 7c shows that the reflectivity of the sample can be reduced to below 5% by KOH etching for 90 min (see SEM images in Figure 7a,b). We assume that the height of the 90 min etched sample could be slightly higher and more tapered than that of the one etched for 50 min, which is difficult to observe from SEM images.

Tapered AR structures can be fabricated at different temperatures and different pHs of KOH solutions. All of these Si structures demonstrate an excellent broad-band antireflective property, which means that the etching conditions for obtaining SWSs are not very strict. For dry etching methods, complicated etching conditions (such as volume ratio of reactive ions, chamber pressure, radio frequency power,[53] etc.) need to be investigated to realize high etching selectivity between Si and masks. There is no need for wet etching. Also, prolonging the etching time cannot decrease the antireflection properties[31] because the etch rate on Si(111) sidewalls is the same after "V"-shaped cross-sectional profiles formed. In our experiments, we just need to consider the effect of etching time on AR properties, so it is much easier and simpler to conduct. However, it should be noted that, for achieving sufficient AR performance, longer etching times are required for relatively lower temperatures. This implies that Si etching is a temperature-dependent process. That is to say, Si is dissolved more quickly in high-temperature solution than in low-temperature solution. In addition, the solubility of the reaction product $Si(OH)_4$ complex may be increased with an increasing temperature.[54] If the reaction products cannot be dissolved into the etching solution sufficiently, the concentration of the orthosilicic acid complex near the silicon surface could be high enough to form a polymer-like layer. When the polymer-like layer decomposes, a residue (such as SiO_2) on the Si surface is produced. These pyrophyllite-type silicates will passivate the Si surface and prevent further etching by the detachment of KOH etching solution.[54] With the same temperature, a longer etching time is needed to achieve good AR performance in a KOH solution at pH 12 than at pH 13. This is because the etching rate reduces with decreasing pH when the KOH concentration is below 5 mM.[55] In addition, $Si(OH)_4$ complex solubility may be higher when the pH of the solution is higher. Considering the AR performance and producing efficiency, we prefer to conduct the etching process at 50 °C in a KOH solution with a pH of 13 for 30 min. With this condition, wafer-scale SWSs are directly patterned on the Si substrate, exhibiting an excellent AR property.

The Fresnel reflection of an incident light comes from the large refractive index discontinuity at the interface of two media. Usually, a multilayer with a stepped refractive index is employed.[4] The large refractive index discontinuity between the two media is split into smaller steps, resulting in a lower reflectivity. According to effective medium theory, SWSs with a pyramidal shape can be considered as a stack of multilayers with an effective refraction index, n_{eff},[31] which exhibits a graded index property. The pyramidal arrays possess antireflective

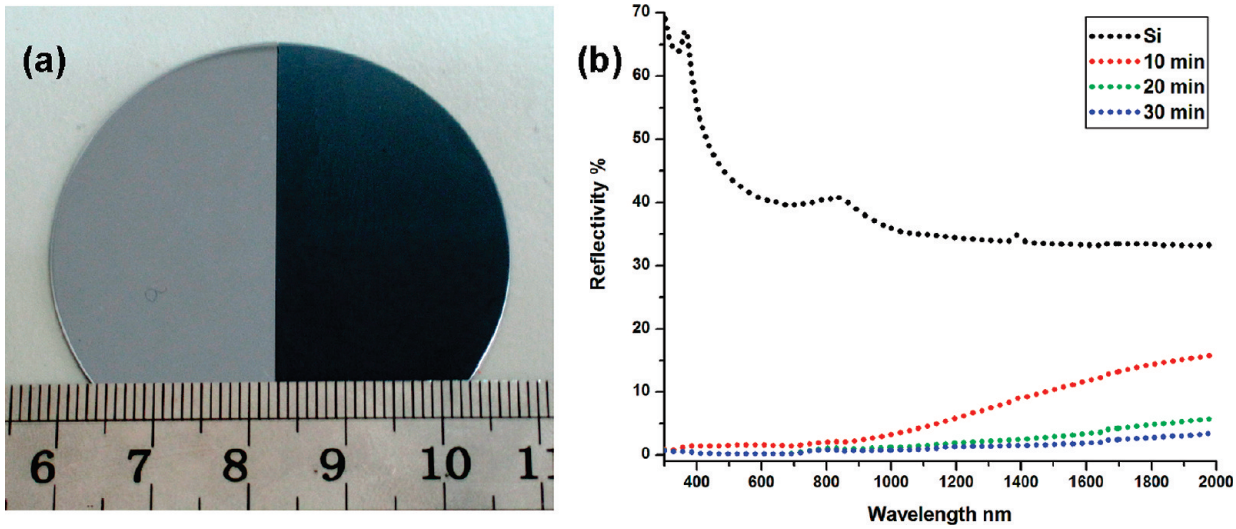

Figure 4. (a) Photograph of an SWS Si wafer etched for 30 min (right part) in a KOH solution with a pH of 13 at 50 °C and the bare Si wafer (left part). (b) Reflectance spectra of SWS Si samples with different etching times in a KOH solution with a pH of 13 at 50 °C. A measured reflectivity for polished Si is shown for comparison.

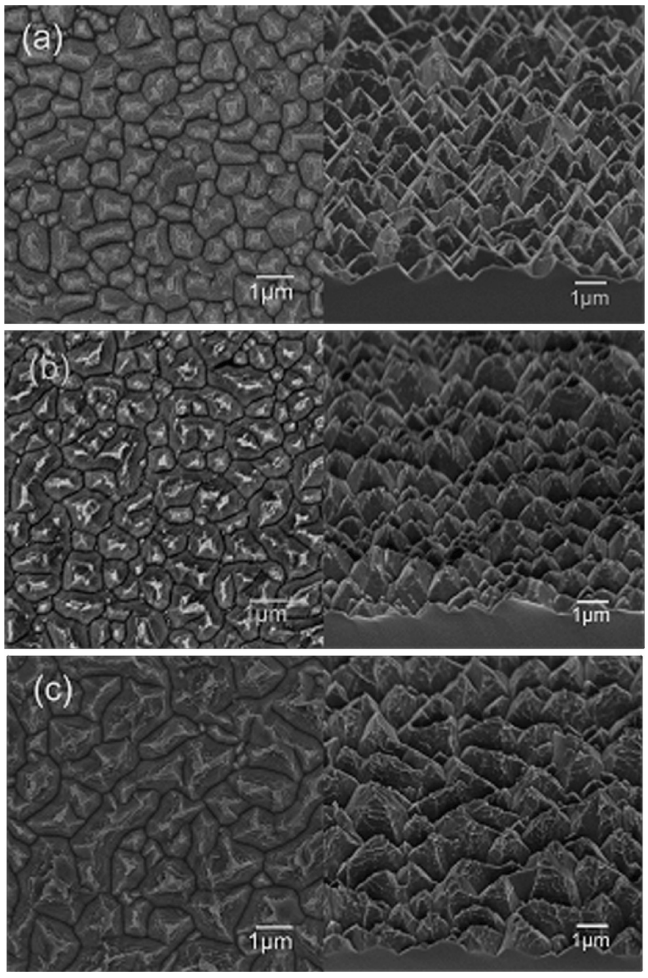

Figure 5. Top-view (left column) and cross-sectional SEM (right column) images for the Si SWS arrays etched in a KOH solution with a pH of 13 with different times at different temperatures: (a) 30 min at 50 °C, (b) 12 h at 25 °C, and (c) 1 h at 38 °C.

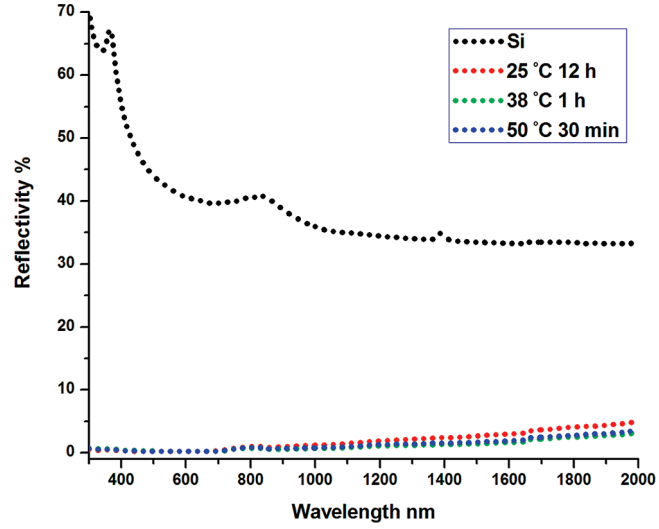

Figure 6. Reflectance spectra of the SWS Si samples with 12 h of etching at 25 °C (red dotted line), 1 h of etching at 38 °C (green dotted line), and 30 min of etching at 50 °C (blue dotted line) in a KOH solution with a pH of 13 and of a polished Si (black dotted line).

character. Theoretically, to achieve the best performance of antireflection with near-zero reflectivity,[31] perfectly tapered SWSs and "V"-shaped profiles of the grooves are required for SWSs. Appropriate SWS heights are also needed for the great suppression of the reflectivity. In the ideal model, the n_{eff} value gradually increases from 1 to n_{Si} from the boundary of air/SWS to the boundary of SWS/Si. In previous investigations, the greatest suppression of reflection happens when the pyramid height (d) to wavelength (λ) ratio is greater than 0.4, and the reflectivity will slightly fluctuate and approach zero by further increasing the aspect ratio d/λ.

As revealed by our experimental measurements, pyramids with flat tops (as presented in Figure 3a and the Supporting Information, Figure S4a) induce an abrupt increase of n_{eff} at the interface of air/array, leading to a higher residual reflection. With further etching, Si pyramids were changed from truncated to tapered ones, so the n_{eff} is approaching 1 at the interface of air/array. From top-view images, there is no flat area at the bottom of neighboring pyramids, which results in the n_{eff} at the interface of array/Si approaching n_{Si}. Therefore, by introducing a continuous refractive index gradient between the air and the Si substrate interface, the tapered arrays can exhibit an excellent broad-band AR property.

As displayed in Figures 5a−c and 7b, the pyramidal structures are not completely the same in morphology. The sample shown

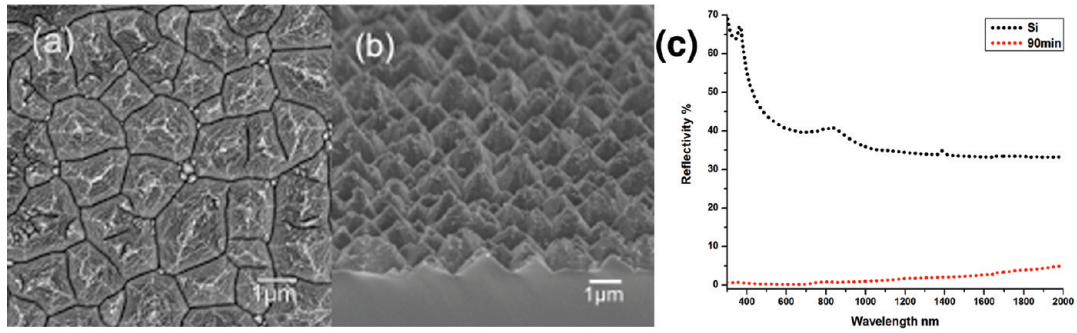

Figure 7. (a) Top-view and (b) cross-sectional SEM images for the Si pyramidal arrays with 90 min of etching in a KOH solution with a pH of 12 at 50 °C. (c) Reflectance spectra of the SWS Si surface with 90 min of etching and a polished Si.

in Figure 5a is relatively tapered compared with others. The sample presented in Figure 5b has the highest density of small pyramids. The dimension of the array shown in Figure 5c is larger and deeper than the others. The SWSs fabricated on Si use OTS islands as selective chemical etching masks, so the morphologies of SWSs are determined by the dimension and density of the islands and etching conditions.[54,55] When the density is low, the dimension of the island and distance between two adjacent islands are large. As shown in Figure 1, the average size of OTS islands is around 1.0 ± 0.15 μm, which means that the size and distance variation between minimum and maximum islands can reach 300 nm. This variation of the island size leads to the difference of etching mask size and, further, the difference of height and size of the Si arrays. As indicated by Figure 5c, when the density of the islands is slightly low, the structures are larger and higher than those in Figure 5a,b. Different dimensions of the arrays would lead to different antireflective performance. With the increasing of the aspect ratio, d/λ, the arrays in Figure 5c exhibit lower reflectivity than others (see Figure 6). However, it does not mean that larger and higher arrays exhibit lower antireflection because the scattering will be enhanced at the same time, which reduces the antireflective property.[56] Therefore, proper dimension and high aspect ratio d/λ can result in excellent antireflection. Schadt et al.,[57] theoretically, have obtained the correlation of the best antireflective wavelength and the periods of SWSs, but no related experimental result has been reported. Further reduction of the reflectivity might be acquired by optimizing the etching conditions and the density and dimensions of OTS islands.

When the fractal OTS monolayers were used as etching masks (without OTMS molecules), no pyramidal structures were produced. Scanning electron microscopy images for samples with different etching times are shown in Figure S5 (see the Supporting Information). Clearly, when the etching time is increased, the fractal OTS monolayers were transferred to Si surfaces, and only main branches remained after 40 min of etching (Figure S5c, Supporting Information); but no Si pyramids were formed. Usually, a gradient refractive index between air and the substrate material can hardly be introduced by these structures because of the minor height of the structure and a large space between two islands. Therefore, the fractal islands are not suitable to be used as etching masks. As mentioned above, no obvious differences of wettability exist in the lonely OTMS monolayers; selective chemical etching was hardly to be realized. The single OTMS films also cannot be used as etching masks.

Recently, we have tried to assemble other mixed SAMs. "Island" structures surrounded by "sea" were also observed when the mixture of OTS and octadecylphosphonic acid (OPA) was assembled on a Si substrate (AFM image is not shown here). The OTS islands were much smaller and denser than the one formed with OTMS SAMs. More detailed investigation is still ongoing. In principle, if the SAM island structures have suitable shape and density and exhibit different wettability in LC islands and LE sea, the films may be used as etching masks, for example, a octadecyltrimethoxysilane and methyl stearate mixed monolayer,[58] OTS and 1*H*,1*H*,2*H*,2*H*-perfluorodecyltrichlorosilane film,[59] behenic acid and partially fluorinated carboxylic acid ether mixed monolayer,[39] and so on. These mixed monolayers are all phase-separated organic SAMs with island structures. If the island regions are formed by the hydrophobic terminal group (such as $-CH_3$ and $-F$) and the sea region is formed by the hydrophilic end group (such as $-OH$, $-COOH$, and $-NH_2$), the films could be much better for being used as etching masks because of the distinct wettability. This research work is still going on in our group.

Conclusion

In summary, a simple and scalable nonlithographic technique is demonstrated for SWS antireflection, in which the mixed self-assembled monolayers consisting of OTS islands are used as chemical etching masks. As a consequence, tapered pyramidal arrays were created, which exhibit consistent low reflection (<3.8%) in both visible and near-infrared wavelengths (300−2000 nm). Optimizing etching conditions and adjusting the density and dimensions of OTS islands will further improve the antireflection performance. This approach is of great technological importance in improving conversion efficiencies of crystalline silicon solar cells and optical devices.

Acknowledgment. Financial support was given by the National Natural Science Foundation of China (20773052), the Program for New Century Excellent Talents in University, the National Basic Research Program (2007CB808003 and 2009CB939701), and the Program 111.

Supporting Information Available: Cross-sectional analysis of AFM for mixed monolayers; SEM images and reflectivity spectra of samples etched in a KOH solution with a pH of 13 at 25 °C for 1 and 5 h, in pH 13 at 38 °C for 10 and 30 min, and in pH 12 at 50 °C for 20 and 50 min; AFM for fractal SAM OTS islands without OTMS and related SEM images of etched samples; and AFM for OTMS films without OTS. This material is available free of charge via the Internet at http://pubs.acs.org.

References and Notes

(1) Striemer, C. C.; Fauchet, P. M. *Appl. Phys. Lett.* **2002**, *81*, 2980–2982.

(2) Lee, Y. J.; Ruby, D. S.; Peters, D. W.; McKenzie, B. B.; Hsu, J. W. P. *Nano Lett.* **2008**, *8*, 1501–1505.
(3) Kanamori, Y.; Ishimori, M.; Hane, K. *IEEE Photonics Technol. Lett.* **2002**, *14*, 1064–1066.
(4) Glaser, T.; Ihring, A.; Morgenroth, W.; Seifert, N.; Schroter, S.; Baier, V. *Microsyst. Technol.* **2005**, *11*, 86–90.
(5) Lee, C.; Bae, S. Y.; Mobasser, S.; Manohara, H. *Nano Lett.* **2005**, *5*, 2438–2442.
(6) Doshi, P.; Jellison, G. E.; Rohatgi, A. *Appl. Opt.* **1997**, *36*, 7826–7837.
(7) Gombert, A.; Glaubitt, W.; Rose, K.; Dreibholz, J.; Blasi, B.; Heinzel, A.; Sporn, D.; Doll, W.; Wittwer, V. *Thin Solid Films* **1999**, *351*, 73–78.
(8) Walheim, S.; Schaffer, E.; Mlynek, J.; Steiner, U. *Science* **1999**, *283*, 520–522.
(9) Kanamori, Y.; Sasaki, M.; Hane, K. *Opt. Lett.* **1999**, *24*, 1422–1424.
(10) Knittl, Z. *Optics of Thin Films*; John Wiley & Sons Press: London, 1976.
(11) Macleod, H. A. *Thin-Film Optical Filters*; Adam Hilger Ltd. Press: London, 1986.
(12) Yoldas, B. E.; Partlow, D. P. *Appl. Opt.* **1984**, *23*, 1418–1424.
(13) Thomas, I. M. *Appl. Opt.* **1988**, *27*, 3356–3358.
(14) Clapham, P. B.; Hutley, M. C. *Nature* **1973**, *244*, 281–282.
(15) Stavenga, D. G.; Foletti, S.; Palasantzas, G.; Arikawa, K. *Proc. R. Soc. London, Ser. B* **2006**, *273*, 661–667.
(16) Lalanne, P.; Morris, G. M. *Nanotechnology* **1997**, *8*, 53–56.
(17) Path, P.; Wileke, G.; Bucher, E.; Szlufcic, J.; Muri, R. M.; Declercq, K.; Nijs, J.; Mertens, R. *Proceedings of the 24th IEEE Photovoltaic Specialist Conference*, HI, 1994.
(18) Kanamori, Y.; Roy, E.; Chen, Y. *Microelectron. Eng.* **2005**, *78*, 287–293.
(19) Hadobás, K.; Kirsch, S.; Carl, A.; Acet, M.; Wassermann, E. F. *Nanotechnology* **2000**, *11*, 161–164.
(20) Aydin, C.; Zaslavsky, A.; Sonek, G. J.; Goldstein, J. *Appl. Phys. Lett.* **2002**, *80*, 2242–2244.
(21) Yu, Z. N.; Gao, H.; Wu, W.; Ge, H. X.; Chou, S. Y. *J. Vac. Sci. Technol., B* **2003**, *21*, 2874–2877.
(22) Zhang, G.; Zhang, J.; Xie, G. Y.; Liu, Z. F.; Shao, H. B. *Small* **2006**, *2*, 1440–1443.
(23) Jansen, H.; Boer, M. D.; Burger, J.; Legtenberg, R.; Elwenspoek, M. *Microelectron. Eng.* **1995**, *27*, 475–480.
(24) Sai, H.; Fujii, H.; Arafune, K.; Ohshita, Y.; Yamaguchi, M.; Kanamori, Y.; Yugami, H. *Appl. Phys. Lett.* **2006**, *88*, 201116.
(25) Sun, C. H.; Min, W. L.; Linn, N. C.; Jiang, P.; Jiang, B. *Appl. Phys. Lett.* **2007**, *91*, 231105.
(26) Sun, C. H.; Jiang, P.; Jiang, B. *Appl. Phys. Lett.* **2008**, *92*, 061112.
(27) Grann, E. B.; Moharam, M. G.; Pommet, D. A. *J. Opt. Soc. Am. A* **1995**, *12*, 333–339.
(28) Southwell, W. H. *J. Opt. Soc. Am. A* **1991**, *8*, 549–553.
(29) Thornton, B. S. *J. Opt. Soc. Am.* **1975**, *65*, 267–270.
(30) Zhao, J.; Green, M. A. *IEEE Trans. Electron Devices* **1991**, *38*, 1925–1934.
(31) Wang, S.; Yu, X. Z.; Fan, H. T. *Appl. Phys. Lett.* **2007**, *91*, 061105.
(32) Kolesar, E. S.; Bright, V. M.; Sowders, D. M. *Thin Solid Films* **1996**, *291*, 23–29.
(33) Hao, J. Y.; Lu, N.; Xu, H. B.; Wang, W. T.; Gao, L. G.; Chi, L. F. *Chem. Mater.* **2009**, *21*, 1802–1805.
(34) Carraro, C.; Yauw, O. W.; Sung, M. M.; Maboudian, R. *J. Phys. Chem. B* **1998**, *102*, 4441–4445.
(35) Bierbaum, K.; Grunze, M.; Baski, A. A.; Chi, L. F.; Schrepp, W.; Fuchs, H. *Langmuir* **1995**, *11*, 2143–2150.
(36) Sung, M. M.; Carraro, C.; Yauw, O. W.; Kim, Y.; Maboudian, R. *J. Phys. Chem. B* **2000**, *104*, 1556–1559.
(37) Bush, B. G.; DelRio, F. W.; Opatkiewicz, J.; Maboudian, R.; Carraro, C. *J. Phys. Chem. A* **2007**, *111*, 12339–12343.
(38) Bhushan, B.; Kulnkar, V. A. V.; Koi., N.; Boehm, M.; Odoni, L.; Martelet, C.; Belin, M. *Langmuir* **1995**, *11*, 3189–3198.
(39) Overney, R. M.; Meyer, E.; Frommer, J.; Güntherodt, H. J. *Langmuir* **1994**, *10*, 1281–1286.
(40) Takano, H.; Fujihira, M. *J. Vac. Sci. Technol., B* **1996**, *14*, 1272–1275.
(41) Lio, A.; Charych, D. H.; Salmeron, M. *J. Phys. Chem. B* **1997**, *101*, 3800–3805.
(42) Fan, F. Q.; Maldarelli, C.; Couzis, A. *Langmuir* **2003**, *19*, 3254–3265.
(43) Harder, P.; Bierbaum, K.; Woell, Ch.; Grunze, M.; Heid, S.; Effenberger, F. *Langmuir* **1997**, *13*, 445–454.
(44) Taut, C.; Pertsin, A.; Grunze, M. *Langmuir* **1996**, *12*, 3481–3489.
(45) Cassie, A. B. D. *Discuss. Faraday Soc.* **1948**, *3*, 11–16.
(46) Choi, I.; Kim, Y.; Kang, S. K.; Lee, J.; Yi, J. *Langmuir* **2006**, *22*, 4885–4889.
(47) Shi, F.; Chen, X. X.; Wang, L. Y.; Niu, J.; Yu, J. H.; Wang, Z. Q.; Zhang, X. *Chem. Mater.* **2005**, *17*, 6177–6180.
(48) Lenhert, S.; Zhang, L.; Mueller, J.; Wiesmann, H. P.; Erker, G.; Fuchs, H.; Chi, L. F. *Adv. Mater.* **2004**, *16*, 619–624.
(49) Chen, X. D.; Lenhert, S.; Hertz, M.; Lu, N.; Fuchs, H.; Chi, L. F. *Acc. Chem. Res.* **2007**, *40*, 393–401.
(50) Hesketh, P. J.; Kieling, V. C.; Gerischer, H. *J. Electrochem. Soc.* **1993**, *140*, 1080–1084.
(51) Schwartz, D. K.; Steinberg, S.; Israelachvili, J.; Zasadzinski, J. A. N. *Phys. Rev. Lett.* **1992**, *69*, 3354–3357.
(52) Kumar, N.; Maldarelli, C.; Steiner, C.; Couzis, A. *Langmuir* **2001**, *17*, 7789–7797.
(53) Xu, H. B.; Lu, N.; Qi, D. P.; Hao, J. Y.; Gao, L. G.; Zhang, B.; Chi, L. F. *Small* **2008**, *11*, 1972–1975.
(54) Sarro, P. M.; Brida, S.; Ashruf, C. M. A.; Vlist, W. V. D.; Zeijl, H. V. *Sens. Mater.* **1998**, *10*, 201–212.
(55) Glembolcki, O. J.; Palik, E. D.; De Guel, G. R.; Kendall, D. L. *J. Electrochem. Soc.* **1991**, *138*, 1055–1063.
(56) Theobald, L.; Michael, H.; Michael, S.; Robert, B.; Joachim, P. S. *Nano Lett.* **2008**, *8*, 1429–1433.
(57) Ibn-Elhaj, M.; Schadt, M. *Nature* **2001**, *410*, 796–799.
(58) Britt, D. W.; Hlady, V. *J. Phys. Chem. B* **1999**, *103*, 2749–2754.
(59) Fang, J. Y.; Knobler, C. M. *Langmuir* **1996**, *12*, 1368–1374.

JP908139H